Biophysical Journal Volume 106 March 2014 1301–1308

Depolarization Laplace Transform Analysis of Exchangeable Hyperpolarized ^{129}Xe for Detecting Ordering Phases and Cholesterol Content of Biomembrane Models

Matthias Schnurr, Christopher Witte, and Leif Schröder*

European Research Council Project BiosensorImaging, Leibniz-Institut für Molekulare Pharmakologie (FMP), Berlin, Germany

ABSTRACT We present a highly sensitive nuclear-magnetic resonance technique to study membrane dynamics that combines the temporary encapsulation of spin-hyperpolarized xenon (^{129}Xe) atoms in cryptophane-A-monoacid (CrA_{ma}) and their indirect detection through chemical exchange saturation transfer. Radiofrequency-labeled Xe@CrA_{ma} complexes exhibit characteristic differences in chemical exchange saturation transfer-driven depolarization when interacting with binary membrane models composed of different molecular ratios of DPPC (1,2-dipalmitoyl-*sn*-glycero-3-phosphocholine) and POPC (1-palmitoyl-2-oleoyl-*sn*-glycero-3-phosphocholine). The method is also applied to mixtures of cholesterol and POPC. The existence of domains that fluctuate in cluster size in DPPC/POPC models at a high (75–98%) DPPC content induces up to a fivefold increase in spin depolarization time τ at 297 K. In POPC/cholesterol model membranes, the parameter τ depends linearly on the cholesterol content at 310 K and allows us to determine the cholesterol content with an accuracy of at least 5%.

INTRODUCTION

The properties of plasma membranes vary widely between different cell types, and even within a single cell, the phospholipid distribution is inhomogeneous (1). Diverse methods have been developed to study the structure and dynamics of membranes. Those methods include, for example, fluorescence techniques (2), differential scanning calorimetry (3), freeze-fracture electron microscopy (4), atomic force microscopy (5), electron spin resonance (6), and nuclear magnet resonance (NMR)-based methods (7). NMR studies benefit from the molecular-specific signature of the acquired signal and take advantage of the detectable nuclei ^{1}H, ^{2}H, ^{13}C, ^{15}N, or ^{31}P and exploit differences in either

1. T_1 or T_2 relaxation times,
2. Chemical shift anisotropy,
3. Isotropic chemical shift, or
4. Order parameters of ^{13}C-^{1}H or ^{13}C-^{2}H bonds.

To obtain sufficient signal from nuclei that have low natural abundance, such as ^{2}H or ^{13}C, the phospholipids must be isotope-labeled. Additionally, selective labeling must be used to prevent undesirable background from these atoms in the acyl chains or in the headgroup of the phospholipids.

The isotope ^{129}Xe (spin 1/2) is also detectable by NMR and is not naturally present in biological tissue. Chemically inert Xe atoms have a high affinity for the hydrophobic core of phospholipid bilayers (8) and it has been demonstrated that hyperpolarizing Xe provides sufficient signal that it can be utilized to discriminate between different types of cells (9), presumably due to their different membrane composition. The complexity of biological membranes makes their direct investigation difficult. Artificially prepared membranes are much easier to examine, yet are still excellent models of biomembranes (10), leading to their extensive use. These model membranes have the advantage that they are, for example, more robust, better manageable, and can be consistently prepared.

Like Xe atoms, hydrophobic cryptophane-A-monoacid (CrA_{ma}) readily partitions into lipid bilayers. Together with Xe it can be used as a biosensor for the presence of phospholipids (11) and can even discriminate between different types of liposomes, where model membranes of unsaturated POPC (1-palmitoyl-2-oleoyl-*sn*-glycero-3-phosphocholine) and saturated DPPC (1,2-dipalmitoyl-*sn*-glycero-3-phosphocholine) have shown efficient uptake of such Xe hosts (12). Lipid bilayers of POPC and DPPC are useful membrane models, as phosphocholines with carbonyl chains of 16 and 18 carbon atoms are the most abundant lipid species in mammalian cells (1).

The chemical exchange saturation transfer technique using hyperpolarized nuclei (Hyper-CEST) (13) takes advantage of the temporary encapsulation of hyperpolarized Xe atoms in the CrA_{ma} hosts (of approximately several milliseconds) to enhance the detection of the hosts by up to a factor of 10^3. The encapsulated Xe atoms are depolarized in a controlled manner using a frequency-selective saturation pulse. The induced signal loss can be detected indirectly by monitoring a change of net magnetization of the much larger spin pool of Xe atoms in aqueous solution (Xe@aq in Fig. 1 *a*). Due to this effective amplification via Hyper-CEST, it is possible to detect CrA_{ma} down to femtomolar concentrations in NMR spectroscopy (14,15) and nanomolar concentrations in magnetic resonance imaging applications (16).

Submitted October 18, 2013, and accepted for publication January 31, 2014.

*Correspondence: lschroeder@fmp-berlin.de

Editor: Klaus Gawrisch.

0006-3495/14/03/1301/8 $2.00

http://dx.doi.org/10.1016/j.bpj.2014.01.041

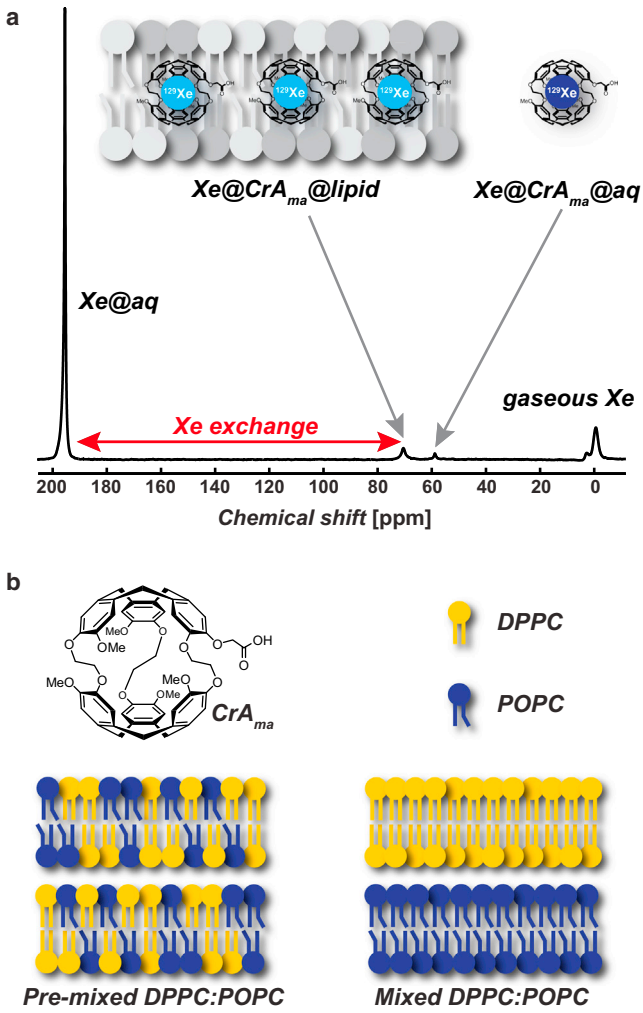

FIGURE 1 (*a*) ^{129}Xe-NMR-spectrum of 1.5 mM POPC and 50 μM CrA_{ma} at 277 K (number of averages $N = 32$). Four of the five Xe pools are detected: Xe in gas phase (0 ppm), Xe@CrA_{ma}@aq (~60 ppm), Xe@CrA_{ma}@lipid (~70 ppm), and Xe@aq (~195 ppm). Xe@lipid usually overlaps with Xe@aq and is not separable. (*b*) Chemical structure of CrA_{ma}. Also depicted are the difference between the premixed and mixed model membranes. To see this figure in color, go online.

In initial experiments with liposomes of pure POPC and pure DPPC, the Hyper-CEST effect was larger for POPC than for DPPC, which was attributed to the different ordering states of the phospholipids (17). This was used to generate novel contrast in magnetic resonance images by analyzing the controlled depolarization due to CEST using an inverse Laplace transform, which we call depolarization Laplace transform analysis (DeLTA). DeLTA has the advantage that no assumption concerning the number of decay processes is needed when analyzing possible multiexponential decays. Here we extend DeLTA to liposomes of defined mixed compositions.

Binary DPPC/POPC mixtures can be organized into a liquid-disordered (L_d) phase, a solid-ordered (S_o) phase, or in a phase where both coexist ($L_d + S_o$) as a function of the concentration ratio and the temperature (3,18) (for a DPPC/POPC phase diagram, see Fig. S1 in the Supporting Material). The L_d phase is characterized by a disordered fluid state, in which the lipids are loosely packed and have a high lateral mobility. In the S_o phase (below 314 K for pure DPPC) the phospholipids are tightly packed, ordered, and have less lateral motion. Recently, Svetlovics et al. (19) observed in experiments and Monte Carlo simulations not only phase separation but also remarkable fluctuations in domain size in the $L_d + S_o$ coexistence phase in DPPC/POPC model membranes.

In this work, we also found indications for the existence of fluctuation in cluster size of the domains in the $L_d + S_o$ coexistence phase using DeLTA. Furthermore, we demonstrate the capability of DeLTA to obtain information about the DPPC/POPC ratio in liposomes and to discriminate the cholesterol level of lipid bilayers. The results of the latter experiment are compared to fluorescence anisotropy measurements of POPC/cholesterol membrane models.

MATERIALS AND METHODS

POPC (1-palmitoyl-2-oleoyl-*sn*-glycero-3-phosphocholine), DPPC (1,2-dipalmitoyl-*sn*-glycero-3-phosphocholine), and a mini-extruder were purchased from Avanti Polar Lipids (Alabaster, AL). Cholesterol and all other chemicals were purchased from Sigma-Aldrich (Steinheim, Germany). The gas mixture used for Xe measurements was 5% Xe (natural abundance, ~26% ^{129}Xe), 10% N_2, and 85% He (Praxair, Biebesheim, Germany).

Liposome preparation

Liposomes were prepared using extrusion (20) as follows: 25 mg/mL POPC, DPPC, and cholesterol were dissolved in MeOH/$CHCl_3$ (1:1). The solutions were mixed to yield the desired molar concentration ratio and the organic solvents were removed in a rotary evaporator (RV 10; IKA, Staufen, Germany) at 40 rpm and 333 K. High-vacuum (10^{-3} mbar) was applied for at least 6 h to remove any possible remaining solvents resulting in a dry, thin lipid film on the glass wall. After hydrating for 15 min with 1.0 mL buffer (10 mM HEPES, 100 mM NaCl, pH 7.3), at 333 K the resulting suspension was subjected to five freeze-thaw cycles (liquid N_2 to 333 K water bath). The obtained suspension was pushed 17 times through polycarbonate membranes (100-nm pore size) using a mini-extruder with heating block (333 K) to obtain homogeneously sized unilamellar vesicles. The size of the vesicles (97 ± 26) nm was measured by dynamic light scattering and the concentration of each stock solution was determined via the Stewart assay (21).

Xenon hyperpolarization

Approximately 25% Xe spin hyperpolarization was obtained using a continuous flow through a custom-designed polarizer (22) via spin exchange optical pumping with rubidium atoms (^{129}Xe flow through cell: 6.47×10^{-3} slm(^{129}Xe)). The electrons of the rubidium atoms were excited using a 150 W continuous-wave diode-laser (795 nm, 0.5-nm bandwidth) at an absolute pressure of 4.5 bar.

NMR setup and Hyper-CEST experiments

NMR experiments were performed using a 9.4 T NMR spectrometer (Bruker Biospin, Ettlingen, Germany). A 10-mm inner diameter double-resonant probe for ^{1}H and ^{129}Xe was used for both excitation and detection.

Using the spectrometer's temperature control unit, the samples were maintained at 297 K for the DPPC/POPC experiment and at 310 K for the POPC/cholesterol experiments. For all experiments, a lipid concentration of 200 μM and CrA_{ma} concentration of 5 μM was used. Before acquiring each data point of a CEST-spectrum, freshly hyperpolarized Xe gas was bubbled for 15 s at 1.85×10^{-3} slm(^{129}Xe) into solution (1.5 mL) inside a 10-mm NMR tube kept under 4.5 bar absolute pressure followed by a 2-s delay to allow remaining bubbles to collapse. The bubbling does not change the sample's target temperature (see Section S3 in the Supporting Material). Each data point of a CEST-spectrum was acquired by irradiating a 10-μT saturation pulse at the desired frequency that lasted for 5 s (8 s in experiments with cholesterol), after which M_z of the Xe@aq resonance (110.7046 MHz $\hat{=}$ 193.3 ppm) was read out. Normalization in all experiments was obtained by dividing M_z by M_{z0}, which is the signal of Xe@aq after off-resonant irradiation (at 315.3 ppm). Sweeping the saturation pulse over a frequency range yields an entire CEST-spectrum. The resonances in the CEST spectra were fitted in the software MATLAB (The MathWorks, Natick, MA) using exponential Lorentzians (ExpLor) (23),

$$\mathrm{ExpLor}(\delta) = \exp\left[-\frac{2A}{\pi}\frac{\gamma^2}{4(\omega_{\mathrm{res}}-\delta)^2+\gamma^2}\right], \qquad (1)$$

in which δ is the chemical shift, γ is related to the width of the resonance in the CEST-spectrum, ω_{res} is the resonance frequency of Xe@CrA_{ma} either in aqueous solution or in lipids, and the remaining on-resonant ($\omega_{\mathrm{res}} = \delta$) magnetization M_z/M_{z0} is determined via parameter A (17). For the DeLTA experiments, the saturation pulse was set to the Xe@CrA_{ma}@lipid resonance frequency determined from the CEST spectra and varied from 10^{-4} to 20 s. The obtained controlled depolarization curves were analyzed using an inverse Laplace transform algorithm based on the MATLAB routine *rilt.m* (24), which yielded the depolarization time constants τ. Therein the smoothing parameter α was set to 0.005. The depolarization time distribution was determined using 120 points logarithmically spaced to cover a large range from 1 to 100 s and fitted with a lognormal distribution. For details concerning the complete algorithm, see Schnurr et al. (17). The performance of DeLTA on simulated data with different noise levels is shown in the Supporting Material.

Fluorescence anisotropy experiments

Fluorescence anisotropy is defined as $\langle r\rangle = (I_{||} - GI_{\perp})/(I_{||} + GI_{\perp})$ (2), where $I_{||}$ and $I_{\perp}$ are the intensities of detected parallel and perpendicular polarized light compared to the irradiated linear polarized light. The G-factor ($0 < G < 1$) is the ratio of sensitivities of the detection system for parallel and perpendicular polarized light, and has to be measured before each experiment to compensate for sensitivity differences between the two detectors. Measurements with DPH (1,6-diphenyl-1,3,5-hexatriene, from Sigma-Aldrich, Steinheim, Germany) were performed on a FP-6500 spectrofluorometer (JASCO Labor-und Datentechnik, Gross-Umstadt, Germany) equipped with excitation and detection linear polarization filters (excitation wavelength: 357.7 nm; detection wavelength: 426.0 nm; both slits: 10 nm; integration time: 1 s; three averages per sample) at 310 K. The model membranes (200 μM in buffer) were incubated with 2 μM DPH for at least 12 h. Samples were heated up to 310 K for at least 30 min before the measurements.

RESULTS AND DISCUSSION

DPPC/POPC mixtures

We studied various mixtures of DPPC/POPC liposomes as model membrane systems using Hyper-CEST spectroscopy and DeLTA. In the first experiment, we mixed DPPC and POPC in different molar ratios before preparing the liposomes (in the following called "premixed liposomes"; see Fig. 1 *b*). In the second experiment, we titrated pure POPC liposomes into a solution containing pure DPPC liposomes (in the following called "mixed liposomes"; see Fig. 1 *b*). All solutions, including the titrated one, contained 5 μM CrA_{ma}.

Premixed DPPC/POPC liposomes

Hyper-CEST spectra

The CEST spectra of Xe encapsulated in CrA_{ma} interacting with premixed DPPC/POPC liposomes at different molar ratios are shown in Fig. 2 *a*. The Xe@CrA_{ma}@aq resonance at 62 ppm was similar in all CEST spectra. The unvarying chemical shift of this resonance confirms that the temperature was the same in all experiments. The slightly lower M_z/M_{z0} with lower DPPC content is due to spillover from the Xe@CrA_{ma}@lipid resonance.

The CEST resonances of Xe@CrA_{ma}@lipid at 73 ppm were different for different DPPC/POPC ratios. For 100% DPPC, with the membrane being in the S_o phase, M_z/M_{z0} was lower than for a DPPC concentration of 98, 95, 91, and 83%, which yielded the weakest CEST responses (larger M_z/M_{z0}). For DPPC concentrations <77%, M_z/M_{z0} decreased monotonically as the DPPC concentration decreased. We assume that the remarkably weak CEST-resonances for DPPC concentrations between 83 and 98% were due to the formation of lipid rafts with fluctuating domain size in the $S_o + L_d$ phase, as observed by measuring and simulating the heat capacity of the DPPC/POPC bilayer (19).

DeLTA

As shown before by Schnurr et al. (17), we can obtain additional information about the Xe@CrA_{ma}@lipid resonance using DeLTA by keeping the saturation frequency fixed at the Xe@CrA_{ma}@lipid resonance and varying the saturation pulse length t_{sat}. The resulting depolarization processes are shown in Fig. 2 *b*. Analyzing those depolarization processes using an inverse Laplace transform gives a single depolarization time for each DPPC/POPC ratio (Fig. 3, *two columns to the left*). The maxima of the continuous depolarization time distributions are the depolarization times τ (plotted as *red circles* in Fig. 4). The depolarization at a concentration of 100% DPPC ($\tau = (14.2 \pm 0.7)$ s) was up to a factor 4.8 faster than the depolarization in liposomes containing a small amount of POPC (98, 95, 91 and 83% DPPC), e.g., $\tau = (69.1 \pm 2.7)$ s at 98%. We hypothesize that the strong increase in depolarization time was caused by fluctuations in cluster size of the domains, which might have perturbed Xe diffusion and exchange in and out of CrA_{ma}, thus resulting in an inefficient CEST-effect.

For decreasing DPPC concentrations below 77% the depolarization became significantly faster, where $\tau = (2.3 \pm 0.1)$ s

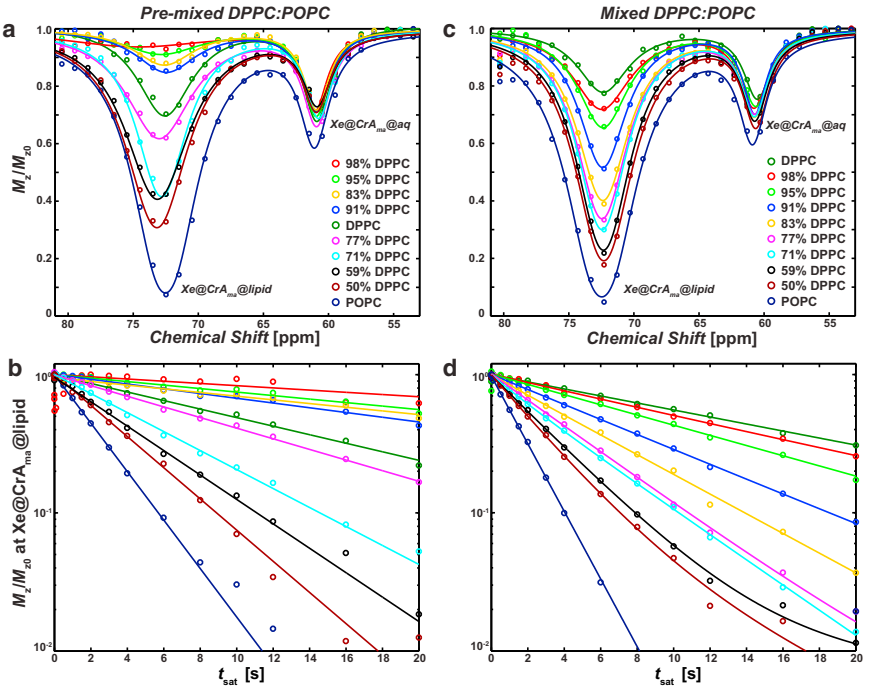

FIGURE 2 CEST spectra of 5 μM CrA_{ma} with 200 μM premixed liposomes (*a*) and mixed liposomes (*c*) at different DPPC/POPC concentration ratios at 297 K. The corresponding depolarization processes when applying a saturation pulse of variable length at the Xe@CrA_{ma}@lipid resonance at 73 ppm are shown in panels *b* and *d*. (*Circles*) Data points; (*solid lines*) fits of the CEST spectra and of the depolarization processes obtained via DeLTA. The first five data points of 98% DPPC in panel *b* were not used in the DeLTA. To see this figure in color, go online.

was the fastest for pure POPC. The ~6-times faster depolarization time in POPC liposomes compared to DPPC liposomes is in very good agreement with our former experiments (17), although the absolute times were different, which we attribute to the different temperature used. The fast depolarization process attributed to POPC was already strongly dominant below 77% DPPC, where $\tau \leq (6.1 \pm 0.4)$ s. This suggests that below 77% DPPC, stable liquid POPC domains of decent size were formed that were dominating the depolarization process and made the remaining DPPC contribution negligible. This domination might be due either to a higher local concentration of CrA_{ma} or a faster exchange rate of Xe atoms in and out of CrA_{ma} in these liquid domains. In addition to the very high depolarization times at high DPPC concentrations (except 100%), it is also interesting that only one depolarization time was found even though domains of different fluidity should coexist (3). Presumably the timescale of the saturation pulse on the order of seconds is much longer than it should take for Xe atoms and CrA_{ma} to diffuse in between the domains, and, therefore, no biexponential depolarization process could be detected, which would present the two coexisting phases. However, to our knowledge, diffusion constants of Xe or CrA_{ma} have not yet been measured in lipid bilayers.

Mixed DPPC/POPC liposomes

Hyper-CEST spectra

At 297 K, pure DPPC or POPC liposomes are far from the phase transition ($S_o \rightarrow L_d$), which takes place at 314 K for DPPC and 271 K for POPC. Furthermore, in lipid bilayers of only one type of phospholipid, no lipid rafts should be formed. We mixed solutions of pure DPPC and POPC liposomes at different molar ratios: first to check if the Hyper-CEST technique is able to sense two different lipids in a solution simultaneously, and second as a control experiment for the phase transition and the fluctuations detected in the premixed liposomes.

The CEST resonances for different DPPC concentrations of Xe@CrA_{ma}@aq at 62 ppm in Fig. 2 *c* again look very similar in all spectra. Additionally, they behaved very similar to the Xe@CrA_{ma}@aq resonances in Fig. 2 *a*, including the spillover of the broad Xe@CrA_{ma}@lipid resonance affecting the Xe@CrA_{ma}@aq resonance at low DPPC concentrations. However, this time the order of the Xe@CrA_{ma}@lipid resonances was different compared to the resonances of premixed liposomes: M_z/M_{z0} decreased monotonically with decreasing DPPC content. Together with the experiment of the premixed liposomes, this indicates that no phase transition was detected. The deviation by ~5% at the resonances' minima of the two CEST spectra of pure DPPC in the premixed and mixed DPPC/POPC liposomes is most likely due to sample preparation. However, qualitatively this does not change the order of the CEST responses.

DeLTA

The corresponding depolarization processes of the Xe@CrA_{ma}@lipid resonance are shown in Fig. 2 *d*. The same strictly monotonic decreasing behavior was found for the depolarization times (Fig. 4) gained from the inverse Laplace transforms (Fig. 3, *two columns to the right*). From

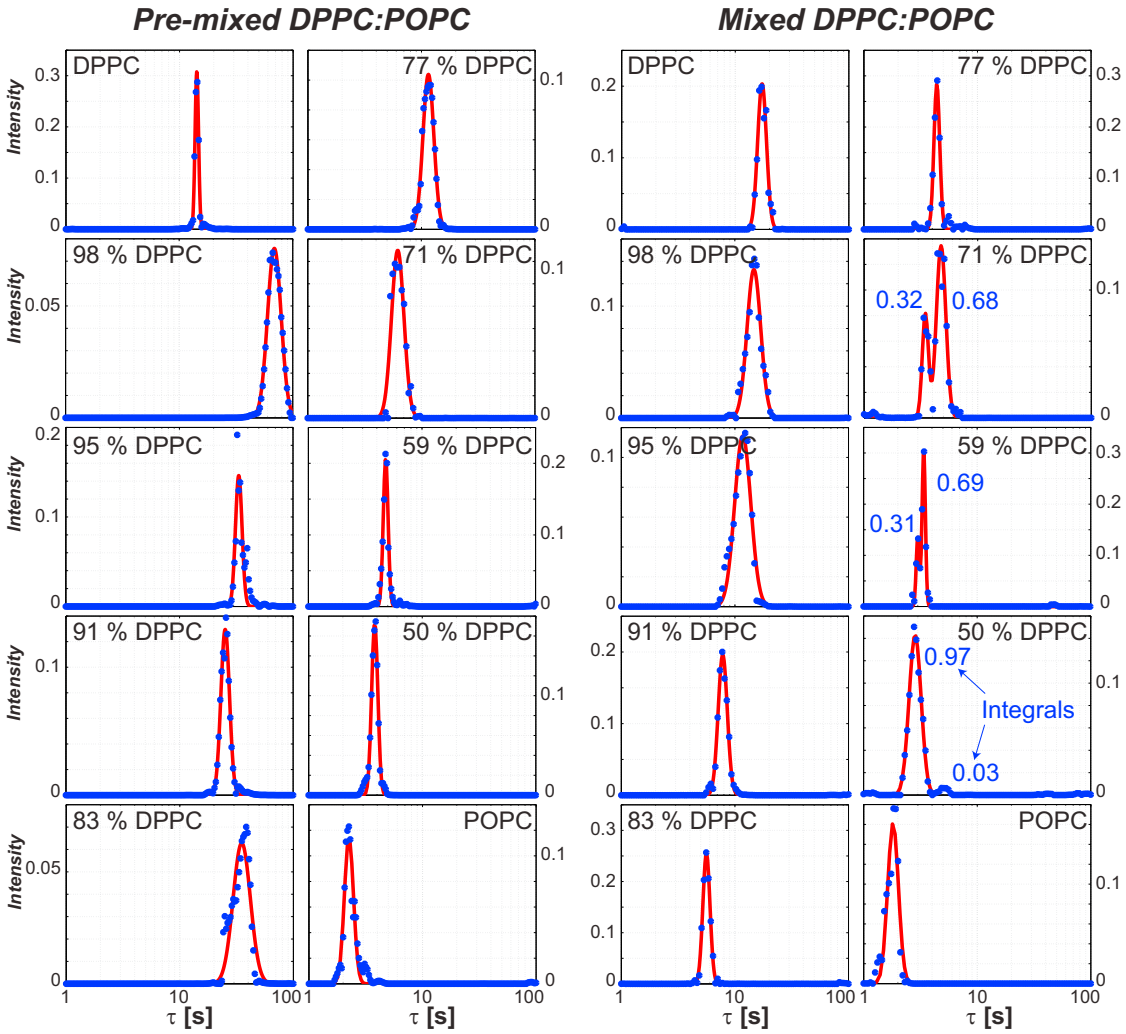

FIGURE 3 Depolarization time distributions obtained via inverse Laplace transform of the depolarization processes shown in Fig. 2, *b* and *d*. Except for DPPC concentrations of 71, 59, and 50% in the mixed DPPC/POPC membrane models, a monoexponential depolarization process was found. Where a biexponential depolarization process was found, the peaks integrals are indicated. To see this figure in color, go online.

this monotonicity, we assume that the different liposomes did not fuse (which might be induced by the bubbling of the gas mixture into the solution) and, as expected, no phase transition was detected.

Interestingly, for high DPPC contents ($\geq$77%), the inverse Laplace transform yielded only one depolarization time τ, whereas, with further decreasing DPPC content (71, 59, 50%), DeLTA yielded a second τ-component (represented in *light blue* and *dark blue* in Fig. 4). The detected biexponential behavior agrees with previous experiments (17) when detecting pure POPC and pure DPPC liposomes in spatially separated compartments. However, in the study presented here, the two depolarization times were shifted compared to τ of pure DPPC and τ of pure POPC. The slower one, τ_2, did not fit as well to τ of pure DPPC as τ_1 fitted to τ of pure POPC. Due to the absence of a physical separation of the two phospholipids, Xe and CrA_{ma} had access to both types of phospholipids with which to interact.

This explains why:

1. The integrals of the peaks' intensities of the depolarization times in Fig. 3 do not represent the concentration ratio of the phospholipids in solution, and
2. The net effect was dominated by the more efficient depolarization process in POPC.

With more quantitative knowledge about the partitioning and the Xe exchange in the different bilayers, one might be able to determine the concentration ratio. By extending the maximal saturation time up to a few τ of pure DPPC, one might resolve the DPPC-related depolarization better and with more accuracy when it has to compete with τ of pure POPC. That only a single, intermediate depolarization time is detected over a large range of DPPC/POPC concentration, might be caused by Xe atoms that travel during one saturation pulse from a POPC liposome to a DPPC liposome.

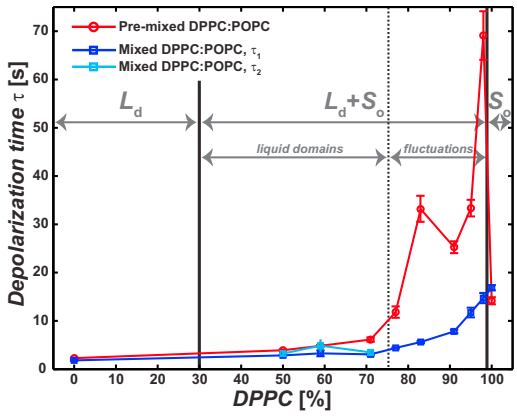

FIGURE 4 Depolarization times τ obtained from the inverse Laplace transforms shown in Fig. 3. The error bars represent the width of the maxima in the depolarization time distributions. The three phases L_d, $L_d + S_o$, and S_o, in premixed liposomes mentioned by Curatolo et al. (3) (see also Fig. S1 in the Supporting Material) are separated (*two solid vertical lines*). The ranges where liquid domains and domains of fluctuating cluster size in the premixed liposomes are assumed (19) are separated (*dashed vertical line*). Two depolarization times τ_1 and τ_2 were found for mixed liposomes at 50, 59, and 71% DPPC concentrations (represented in *dark* and *light blue*). To see this figure in color, go online.

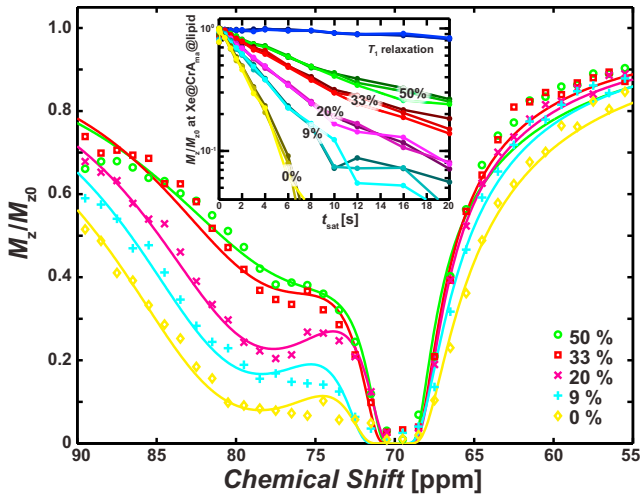

FIGURE 5 CEST spectra of POPC/cholesterol liposomes at 310 K. The cholesterol level is given in %. Resonance at 70 ppm corresponds to Xe@CrA_{ma}@aq; resonance at 77 ppm corresponds to Xe@CrA_{ma}@lipid. (*Inset*) Depolarization of the POPC/cholesterol liposomes with variable saturation time t_{sat} at Xe@CrA_{ma}@lipid (77 ppm in the CEST spectrum). For each cholesterol concentration, three independent measurements were performed. The T_1 relaxation is obtained with applying saturation pulses at −77 ppm. To see this figure in color, go online.

POPC/cholesterol mixtures

In addition to an L_d and S_o phase, a liquid-ordered (L_o) phase can exist in lipid bilayers (25). For example, incorporating cholesterol in POPC bilayers increases the ordering of the acyl chains (26) and promotes the formation of the L_o phase, which implies a reduction in the passive permeability of lipid bilayers (27). However, this ordered phase possesses a high lateral mobility, as does the L_d phase in pure POPC liposomes, and is therefore called the L_o phase (18,28). Although different studies yielded slightly different results (29), basically, at 310 K, a cholesterol concentration of <15% results in an L_d phase. At ~15–45%, the L_d and L_o phases coexist, whereas at higher cholesterol concentrations, only the L_o phase is present. When both phases coexist simultaneously, lipid rafts of the L_o phase are formed (30,31).

Hyper-CEST spectra and DeLTA

We investigated the influence of cholesterol content of POPC bilayers (in the biologically relevant range of 0–50%) on the Xe@CrA_{ma}@lipid resonance using CEST spectroscopy (see Fig. 5, acquired at 310 K). The CEST resonances at 70 ppm were from Xe@CrA_{ma}@aq, and the ones at ~77 ppm arose from Xe@CrA_{ma}@lipid. The latter CEST resonances clearly became weaker with increasing cholesterol level. The Xe@CrA_{ma}@aq resonance was completely saturated for all measured cholesterol levels with the saturation power and saturation time used. However, the resonance's right shoulder did not change with changing the cholesterol level as much as the Xe@CrA_{ma}@lipid resonance, from which we conclude that the Xe@CrA_{ma}@aq resonance did not change significantly. The broad overlap of the two resonances was due to the fast exchange of Xe atoms at 310 K (11,15,32). Further effects caused by raising the temperature from room temperature to 310 K were:

1. M_z/M_{z0} of Xe@CrA_{ma}@aq got lower than M_z/M_{z0} of Xe@CrA_{ma}@lipid, and
2. Both resonances were shifted downfield, whereas the chemical shift of the Xe@CrA_{ma}@aq resonance was more sensitive to a change in temperature than the chemical shift of the Xe@CrA_{ma}@lipid resonance (62 → 70 ppm and 74 →77 ppm, respectively).

The trends are consistent with previous Xe-biosensor data taken of pure POPC and DPPC liposomes (12).

In addition to the CEST spectra, we also applied variable length saturation pulses to the Xe@CrA_{ma}@lipid resonance and performed DeLTA (*inset* in Fig. 5) as in the previous experiments. We verified the accuracy and reproducibility of the method by repeating each measurement three times. A single maximum in the depolarization time distribution was found using DeLTA. The corresponding depolarization times are plotted in Fig. 6 *a*. The depolarization times range from (2.4 ± 0.2) for pure POPC to (8.9 ± 0.3) s for 50% cholesterol, and seem to depend linearly on the cholesterol content. Taking the error bars into account, it should be possible to discriminate the amount of cholesterol in POPC liposomes with an accuracy of at least 5%.

Fluorescence anisotropy

Steady-state fluorescent approaches such as fluorescence anisotropy ($\langle r \rangle$), using DPH as a fluorescent probe, are well-established methods to obtain information concerning

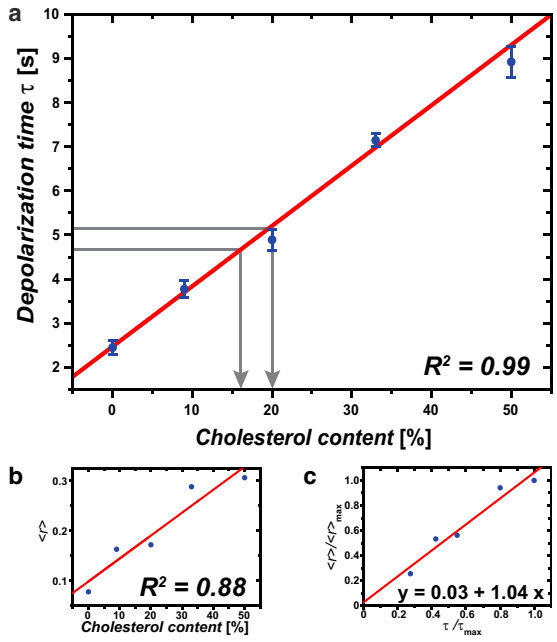

FIGURE 6 (*a*) Depolarization times of the depolarization processes for the POPC/cholesterol liposomes shown in Fig. 5. The depolarization time appears to depend linearly on the cholesterol level in the measured range. From the relatively small error bars the cholesterol level can be determined with an accuracy >5% (*gray arrows*). The error bars represent the standard deviation when analyzing the three depolarization processes from Fig. 5. (*b*) Corresponding fluorescence anisotropy measurements. In both plots the adjusted R^2 values of the linear fits are given. (*c*) Hyper-CEST method is compared with the fluorescence anisotropy method (both normalized to their maximum) yielding a linear dependence of $y = (0.03 \pm 0.09) + (1.04 \pm 0.14)x$. To see this figure in color, go online.

the fluidity of membranes (2). The higher the fluidity of a membrane, the higher the rotational diffusion rate of the fluorescent probe, which exhibits a faster decay of $\langle r \rangle$. Hence, $\langle r \rangle$ is sensitive to the packing of the acyl chains of phospholipids and cholesterol, and can therefore also be used to sense the presence of cholesterol.

The measured $\langle r \rangle$ of the different POPC/cholesterol liposomes is shown in Fig. 6 *b*. Both the depolarization times and $\langle r \rangle$ appear to increase linearly with increasing cholesterol content, and are qualitatively in very good agreement to what has been measured at 296 K in Arora et al. (33) using DPH or at 313 K in Reyes Mateo et al. (28) using *trans*-parinaric acid as a fluorescent probe. However, the noise of the Hyper-CEST data (adjusted $R^2 = 0.99$) is smaller compared to the measurements of $\langle r \rangle$ (adjusted $R^2 = 0.88$). Fig. 6 *c* compares the sensitivities of both methods. The linear fit yields for the *y* axis intercept 0.03 ± 0.09 and 1.04 ± 0.14 for the slope. The slope (≈ 1) illustrates that the two methods possess similar sensitivities by covering a similar dynamical range.

CONCLUSIONS

In this study, we demonstrated that it is possible to obtain information related to the composition of DPPC/POPC and POPC/cholesterol model membranes using Hyper-CEST and DeLTA NMR experiments. The results are in good agreement with studies performed on the same model systems using other, established methods. We have shown that with the Hyper-CEST technique it is possible to discriminate the different compositions of the model membranes. In all presented experiments, acquiring the depolarization curves and analyzing them using an inverse Laplace transform yielded additional information that was not accessible using only a CEST-spectrum. For example, we saw evidence that supports the presence of domains that fluctuate in cluster-size close to the phase transition ($L_d + S_o \rightarrow S_o$) in DPPC/POPC liposomes, as reported by Svetlovics et al. (19). In addition to that, we could discriminate the cholesterol content of liposomes with an accuracy of 5%. The concentrations of both lipids and CrA used in the experiments were low compared to other NMR studies, which have to use at least mM concentrations (7). Nevertheless, the concentrations used not only yielded sufficient signal but can be pushed further before the detection limit is reached. Furthermore, no chemical synthesis or isotope labeling, with, for example, ^{13}C, is necessary to introduce a highly sensitive NMR label into membranes. Therefore, we envision that NMR using hyperpolarized ^{129}Xe will become an integral part of future biomembrane studies, especially when studying systems to which optical approaches are not applicable due to their limitation in penetration depth.

SUPPORTING MATERIAL

Nine equations, three figures, references (34,35), and additional supplemental information, are available at http://www.biophysj.org/biophysj/supplemental/S0006-3495(14)00144-1.

This work was supported by the European Research Council under the European Community's Seventh Framework Program (No. FP7/2007-2013)/European Research Council grant agreement no. 242710 and the Human Frontier Science Program. We thank the Experimental Nuclear Magnetic Resonance Conference committee together with Suraj Manrao for generous support, enabling M.S. to present parts of this work at the 54th Experimental Nuclear Magnetic Resonance Conference.

REFERENCES

1. Lipowsky, R., and E. Sackmann. 1995. Structure and Dynamics of Membranes: I. From Cells to Vesicles/II. Generic and Specific Interactions. Elsevier, New York.
2. Lakowicz, J. R. 2006. Principles of Fluorescence Spectroscopy. Springer, New York.
3. Curatolo, W., B. Sears, and L. J. Neuringer. 1985. A calorimetry and deuterium NMR study of mixed model membranes of 1-palmitoyl-2-oleylphosphatidylcholine and saturated phosphatidylcholines. *Biochim. Biophys. Acta.* 817:261–270. *http://www.sciencedirect.com/science/article/pii/0005273685900276.*
4. Verkleij, A., R. Zwaal, …, L. van Deenen. 1973. The asymmetric distribution of phospholipids in the human red cell membrane. A combined study using phospholipases and freeze-etch electron microscopy.

Biochim. Biophys. Acta. 323:178–193. http://www.sciencedirect.com/science/article/pii/0005273673901430.

5. Rinia, H. A., M. M. Snel, …, B. de Kruijff. 2001. Visualizing detergent resistant domains in model membranes with atomic force microscopy. *FEBS Lett.* 501:92–96. http://www.sciencedirect.com/science/article/pii/S0014579301026369.
6. Marsh, D. 2010. Electron spin resonance in membrane research: protein-lipid interactions from challenging beginnings to state of the art. *Eur. Biophys. J.* 39:513–525. http://link.springer.com/article/10.1007/s00249-009-0512-3.
7. Leftin, A., and M. F. Brown. 2011. An NMR database for simulations of membrane dynamics. *Biochim. Biophys. Acta.* 1808:818–839. http://www.sciencedirect.com/science/article/pii/S0005273610004128.
8. Booker, R. D., and A. K. Sum. 2013. Biophysical changes induced by xenon on phospholipid bilayers. *Biochim. Biophys. Acta.* 1828:1347–1356. http://www.sciencedirect.com/science/article/pii/S0005273613000291.
9. Boutin, C., H. Desvaux, …, P. Berthault. 2011. Hyperpolarized 129Xe NMR signature of living biological cells. *NMR Biomed.* 24:1264–1269. http://onlinelibrary.wiley.com/doi/10.1002/nbm.1686/abstract.
10. Faller, R. 2009. Biomembrane Frontiers: Nanostructures, Models, and the Design of Life. Springer, New York.
11. Meldrum, T., L. Schröder, …, A. Pines. 2010. Xenon-based molecular sensors in lipid suspensions. *J. Magn. Reson.* 205:242–246. http://www.sciencedirect.com/science/article/pii/S1090780710001485.
12. Sloniec, J., M. Schnurr, …, A. Hennig. 2013. Biomembrane interactions of functionalized cryptophane-A: combined fluorescence and 129Xe NMR studies of a bimodal contrast agent. *Chemistry.* 19:3110–3118. http://onlinelibrary.wiley.com/doi/10.1002/chem.201203773/abstract.
13. Schröder, L., T. J. Lowery, …, A. Pines. 2006. Molecular imaging using a targeted magnetic resonance hyperpolarized biosensor. *Science.* 314:446–449. http://www.sciencemag.org/content/314/5798/446.
14. Bai, Y., P. A. Hill, and I. J. Dmochowski. 2012. Utilizing a water-soluble cryptophane with fast xenon exchange rates for picomolar sensitivity NMR measurements. *Anal. Chem.* 84:9935–9941. http://dx.doi.org/10.1021/ac302347y.
15. Schröder, L., T. Meldrum, …, A. Pines. 2008. Temperature response of ^{129}Xe depolarization transfer and its application for ultrasensitive NMR detection. *Phys. Rev. Lett.* 100:257603. http://link.aps.org/doi/10.1103/PhysRevLett.100.257603.
16. Kunth, M., J. Döpfert, …, L. Schröder. 2012. Optimized use of reversible binding for fast and selective NMR localization of caged xenon. *Angew. Chem. Int. Ed. Engl.* 51:8217–8220. http://onlinelibrary.wiley.com/doi/10.1002/anie.201202481/abstract.
17. Schnurr, M., C. Witte, and L. Schröder. 2013. Functionalized ^{129}Xe as a potential biosensor for membrane fluidity. *Phys. Chem. Chem. Phys.* 15:14178–14181. http://pubs.rsc.org/en/content/articlelanding/2013/cp/c3cp51227d.
18. Veatch, S. L., and S. L. Keller. 2003. Separation of liquid phases in giant vesicles of ternary mixtures of phospholipids and cholesterol. *Biophys. J.* 85:3074–3083. http://www.ncbi.nlm.nih.gov/pmc/articles/PMC1303584/.
19. Svetlovics, J. A., S. A. Wheaten, and P. F. Almeida. 2012. Phase separation and fluctuations in mixtures of a saturated and an unsaturated phospholipid. *Biophys. J.* 102:2526–2535. http://www.sciencedirect.com/science/article/pii/S0006349512004614.
20. MacDonald, R. C., R. I. MacDonald, …, L.-r. Hu. 1991. Small-volume extrusion apparatus for preparation of large, unilamellar vesicles. *Biochim. Biophys. Acta.* 1061:297–303. http://www.sciencedirect.com/science/article/pii/000527369190295J.
21. Stewart, J. C. M. 1980. Colorimetric determination of phospholipids with ammonium ferrothiocyanate. *Anal. Biochem.* 104:10–14. http://www.sciencedirect.com/science/article/pii/0003269780902699.
22. Witte, C., M. Kunth, …, L. Schröder. 2012. Hyperpolarized xenon for NMR and MRI applications. *J. Visual. Exper.*. http://www.jove.com/video/4268/hyperpolarized-xenon-for-nmr-and-mri-applications
23. Zaiss, M., M. Schnurr, and P. Bachert. 2012. Analytical solution for the depolarization of hyperpolarized nuclei by chemical exchange saturation transfer between free and encapsulated xenon (HyperCEST). *J. Chem. Phys.* 136:144106–144110. http://jcp.aip.org/resource/1/jcpsa6/v136/i14/p144106_s1.
24. Marino, I.-G. 2007. Rilt.m. The MathWorks, Natick, MA. http://www.mathworks.com/matlabcentral/fileexchange/6523-rilt/content/rilt. [Accessed Oct. 17, 2013].
25. Ahmed, S. N., D. A. Brown, and E. London. 1997. On the origin of sphingolipid/cholesterol-rich detergent-insoluble cell membranes: physiological concentrations of cholesterol and sphingolipid induce formation of a detergent-insoluble, liquid-ordered lipid phase in model membranes. *Biochemistry.* 36:10944–10953. http://dx.doi.org/10.1021/bi971167g.
26. Lafleur, M., P. R. Cullis, and M. Bloom. 1990. Modulation of the orientational order profile of the lipid acyl chain in the *Lα* phase. *Eur. Biophys. J.* 19:55–62. http://link.springer.com/article/10.1007/BF00185086.
27. Xiang, T. X., and B. D. Anderson. 1997. Permeability of acetic acid across gel and liquid-crystalline lipid bilayers conforms to free-surface-area theory. *Biophys. J.* 72:223–237. http://www.sciencedirect.com/science/article/pii/S0006349597786612.
28. Reyes Mateo, C., A. Ulises Acuña, and J. C. Brochon. 1995. Liquid-crystalline phases of cholesterol/lipid bilayers as revealed by the fluorescence of trans-parinaric acid. *Biophys. J.* 68:978–987. http://www.ncbi.nlm.nih.gov/pmc/articles/PMC1281821/.
29. Marsh, D. 2010. Liquid-ordered phases induced by cholesterol: a compendium of binary phase diagrams. *Biochim. Biophys. Acta.* 1798:688–699. http://www.sciencedirect.com/science/article/pii/S0005273610000027.
30. Rietveld, A., and K. Simons. 1998. The differential miscibility of lipids as the basis for the formation of functional membrane rafts. *Biochim. Biophys. Acta.* 1376:467–479. http://www.sciencedirect.com/science/article/pii/S0304415798000197.
31. Simons, K., and E. Ikonen. 1997. Functional rafts in cell membranes. *Nature.* 387:569–572. http://www.nature.com/nature/journal/v387/n6633/full/387569a0.html.
32. Schröder, L., L. Chavez, …, A. Pines. 2008. Temperature-controlled molecular depolarization gates in nuclear magnetic resonance. *Angew. Chem. Int. Ed. Engl.* 47:4316–4320. http://onlinelibrary.wiley.com/doi/10.1002/anie.200800382/abstract.
33. Arora, A., H. Raghuraman, and A. Chattopadhyay. 2004. Influence of cholesterol and ergosterol on membrane dynamics: a fluorescence approach. *Biochem. Biophys. Res. Commun.* 318:920–926. http://www.sciencedirect.com/science/article/pii/S0006291X04008630.
34. Bartik, K., M. Luhmer, …, J. Reisse. 1998. ^{129}Xe and ^{1}H NMR study of the reversible trapping of xenon by cryptophane-A in organic solution. *J. Am. Chem. Soc.* 120:784–791. http://dx.doi.org/10.1021/ja972377j.
35. Fogarty, H. A., P. Berthault, …, J.-P. Dutasta. 2007. A cryptophane core optimized for xenon encapsulation. *J. Am. Chem. Soc.* 129:10332–10333. http://dx.doi.org/10.1021/ja073771c.